

Ferrocene-based sulfonyl dihydropyrazole derivatives: Synthesis, structure, electrochemistry and effect on thermal decomposition of NH_4ClO_4



Ji-Bin Zhuo^a, Heng-Dong Li^a, Cai-Xia Lin^a, Li-Li Xie^{a,b}, Sha Bai^c, Yao-Feng Yuan^{a,b,*}

^a Department of Chemistry, Fuzhou University, Fuzhou 350108, China

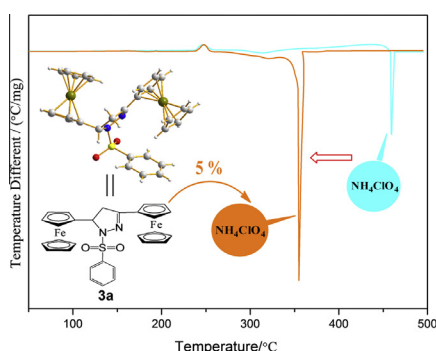
^b State Key Laboratory of Photocatalysis on Energy and Environment, Fuzhou University, Fuzhou 350002, China

^c Beth Israel Deaconess Medical Center (BIDMC), Harvard Medical School, Boston, MA 02215, USA

HIGHLIGHTS

- Three ferrocene-based sulfonyl-substituted dihydropyrazoles **3a–c** are synthesized in moderate yields.
- Molecular structure of **3a** has been characterized by single-crystal X-ray diffraction analysis for a first time.
- The electrochemical behaviors of **3a–c** are discussed; the electrochemical inequivalence of **3a** was confirmed by DFT.
- Dinuclear ferrocenyl pyrazole **3a** shows a greater catalytic effect on the decomposition temperature of AP than **3b–c**.

GRAPHICAL ABSTRACT



ARTICLE INFO

Article history:

Received 30 December 2013

Received in revised form 7 March 2014

Accepted 10 March 2014

Available online 25 March 2014

Keywords:

Dihydropyrazole
Ferrocene
Sulfonyl
Structure
Electrochemistry
Ammonium perchlorate

ABSTRACT

Three ferrocene-based sulfonyl-substituted dihydropyrazoles **3a–c** have been synthesized, from the corresponding α,β -unsaturated diketones, and fully characterized. The crystal structures of **3a–c** have been confirmed by X-ray crystallography, and electrochemistry behaviors of **3a–c** have been examined by cyclic voltammetry (CV). Representatively, the mechanism of the electron transfer in redox process of **3a** has been verified by density functional theory (DFT) calculation. It has been found that the activity of catalytic decomposition of ammonium perchlorate (AP) is significantly lowered (by 62.9–104.7 °C) with an addition of **3a–c**. We expect that the ferrocene-based sulfonyl dihydropyrazole derivatives would have a great value in burning rate catalyst as composite solid propellants.

© 2014 Elsevier B.V. All rights reserved.

Introduction

Pyrazole and its derivatives are widely used in the field of medicine and pesticide [1–7]. Different substituents are introduced to

the pyrazole ring to deliver the corresponding derivatives with alternative functions used in electrochemical sensors [8–10], molecular recognitions [11–13] and decomposition catalysts [14,15]. Specifically, ferrocene has unique aromatic electron-rich potential and electrochemical reversibility [16,17]. Its derivatives have many advantages, including good mobility, flammability, high molecular weight and thermal stability, compared to the traditional combustion catalysts [18,19]. Currently, researchers

* Corresponding author at: Department of Chemistry, Fuzhou University, Fuzhou 350108, China. Tel./fax: +86 591 22866161.

E-mail address: yaofeng_yuan@fzu.edu.cn (Y.-F. Yuan).

Table 1
Crystallographic data and structure refinement parameters of **3a–c**.

Compound	3a	3b	3c
Empirical formula	C ₂₉ H ₂₆ Fe ₂ N ₂ O ₂ S	C ₂₅ H ₂₁ BrFeN ₂ O ₂ S	C ₂₅ H ₂₂ FeN ₂ O ₂ S
Formula weight	578.29	549.26	470.37
Temperature (K)	293(2)	293(2)	293(2)
Wavelength (Å)	0.71073	0.71073	0.71073
Crystal system	Monoclinic	Monoclinic	Orthorhombic
Space group	P2(1)/c	P2(1)/c	P2(1)2(1)2(1)
a (Å)	19.586(4)	13.087(3)	5.9466(12)
b (Å)	10.936(2)	9.844(2)	11.653(2)
c (Å)	11.649(2)	17.752(4)	31.274(6)
α (°)	90.00	90.00	90.00
β (°)	92.71(3)	99.42(3)	90.00
γ (°)	90.00	90.00	90.00
V (Å ³)	2492.4(9)	2256.2(8)	2167.2(8)
Z	4	4	4
D _{calc} (g cm ⁻³)	1.541	1.617	1.442
Absorption coefficient (mm ⁻¹)	1.278	2.558	0.817
F(000)	1472	1112.0	1280
Crystal size (mm)	0.25 × 0.25 × 0.20	0.30 × 0.25 × 0.20	0.50 × 0.30 × 0.20
Index ranges	−22 ≤ h ≤ 25 −13 ≤ k ≤ 14 −14 ≤ l ≤ 15	−15 ≤ h ≤ 13 −11 ≤ k ≤ 11 −21 ≤ l ≤ 21	−7 ≤ h ≤ 7 −15 ≤ k ≤ 15 −38 ≤ l ≤ 40
Reflections collected	20,546	15,470	18,264
Independent reflections	5163 [R(int) = 0.0495]	3462 [R(int) = 0.0660]	4625 [R(int) = 0.0516]
θ range for data collection	3.24–27.55°	3.14–25.00°	3.14–27.51°
Absorption correction	Multi-scan	Multi-scan	Multi-scan
Refinement method	Full-matrix least-squares on F ²	Full-matrix least-squares on F ²	Full-matrix least-squares on F ²
Goodness-of-fit on F ²	1.274	1.296	1.170
Data/restraints/parameters	5709/0/325	3972/0/289	4947/0/280
Final R indices [I > 2σ(I)]	R ₁ = 0.0706 wR ₂ = 0.2127	R ₁ = 0.0803 wR ₂ = 0.2321	R ₁ = 0.0509 wR ₂ = 0.1421
R indices (all data)	R ₁ = 0.0847 wR ₂ = 0.2495	R ₁ = 0.1031 wR ₂ = 0.2700	R ₁ = 0.0573 wR ₂ = 0.1611

689. ¹H NMR (400 MHz, CDCl₃): δ 7.93 (d, *J* = 6.8 Hz, 2H, Ph-H), 7.54 (d, *J* = 6.8 Hz, 3H, Ph-H), 4.92 (s, 1H, Pz-H) (Pz: parazole), 4.76 (d, 1H, Cp-H) (Cp: cyclopentadiene), 4.57 (d, 1H, Cp-H), 4.42 (d, 2H, Cp-H), 4.22 (m, 9H, Cp-H), 4.00 (s, 5H, Cp-H), 3.29 (m, 2H, Pz-H). ¹³C NMR (100 MHz, CDCl₃): δ 160.21 (Pz-C), 137.01 (Ph-C), 133.06 (Ph-C), 128.65 (Ph-C), 128.61 (Ph-C), 74.30 (Cp-C), 70.79 (Cp-C), 70.38 (Cp-C), 69.53 (Cp-C), 69.15 (Cp-C), 68.64 (Cp-C), 67.53 (Cp-C), 59.67 (Pz-C), 43.02 (Pz-C). MS (ESI) *m/z*: [M + H] 578.92, [M⁺] calcd. 578.28. Anal. calcd. for C₂₉H₂₆Fe₂N₂O₂S: C 60.30, H 4.61, N 5.09; found: C 60.23, H 4.53, N 4.84.

Synthesis of 1-phenylsulfonyl-3-ferrocenyl-5-(4-bromophenyl)-4,5-dihydropyrazole (3b)

The complex was prepared by manner analogous of that of **3a**. A yellow powder **3b** (0.48 g, 39%) was obtained after silica gel chromatography. M.p. 265–266 °C (CH₂Cl₂/PE). IR (KBr), ν/cm⁻¹: 3442, 3088, 2917, 1599, 1487, 1447, 1352, 1167, 1107, 822, 719, 689. ¹H NMR (400 MHz, CDCl₃): δ 7.96 (m, *J* = 6.8 Hz, 2H, Ph-H), 7.60 (m, *J* = 6.8 Hz, 3H, Ph-H), 7.53 (d, *J* = 8.0 Hz, 2H, Ph-H), 7.34 (d, *J* = 8.0 Hz, 2H, Ph-H), 4.83 (m, *J* = 11.2, 9.2 Hz, 1H, Pz-H), 4.70 (s, 1H, Cp-H), 4.51 (s, 1H, Cp-H), 4.40 (d, 2H, Cp-H), 3.97 (s, 5H, Cp-H), 3.39 (d, *J* = 17.2, 11.2 Hz, 1H, Pz-H), 2.96 (d, *J* = 17.2, 9.2 Hz, 1H, Pz-H). ¹³C NMR (100 MHz, CDCl₃): δ 159.15 (Pz-C), 140.89 (Ph-C), 135.59 (Ph-C), 133.41 (Ph-C), 132.01 (Ph-C), 128.84 (Ph-C), 128.80 (Ph-C), 128.37 (Ph-C), 121.98 (Ph-C), 69.75 (Cp-C), 67.19 (Cp-C), 64.00 (Pz-C), 45.10 (Pz-C). MS (ESI) *m/z*: [M + H] 549.00, [M⁺] calcd. 549.26. Anal. calcd. for C₂₅H₂₁BrFeN₂O₂S: C 54.74, H 4.03, N 4.99; found: C 54.67, H 3.85, N 5.10.

Synthesis of 1-phenylsulfonyl-3-ferrocenyl-5-benzoyl-4,5-dihydro-1H-pyrazole (3c)

The complex was prepared by manner analogous of that of **3a**. A yellow powder **3c** (0.64 g, 48%) was obtained after silica gel chro-

matography. M.p. 203–204 °C (CH₂Cl₂/PE). IR (KBr), ν/cm⁻¹: 3062, 2926, 1596, 1485, 1446, 1351, 1171, 828, 763, 699. ¹H NMR (400 MHz, CDCl₃): δ 7.98 (d, *J* = 6.8 Hz, 2H, Ph-H), 7.59 (m, *J* = 6.8 Hz, 3H, Ph-H), 7.46 (m, *J* = 7.2 Hz, 2H, Ph-H), 7.41 (t, *J* = 7.2 Hz, 2H, Ph-H), 7.35 (t, *J* = 7.2 Hz, 1H, Ph-H), 4.88 (m, *J* = 11.2, 9.2 Hz, 1H, Pz-H), 4.70 (s, 1H, Cp-H), 4.53 (s, 1H, Cp-H), 4.40 (d, 2H, Cp-H), 3.98 (s, 5H, Cp-H), 3.38 (d, *J* = 17.2, 11.2 Hz, 1H, Pz-H), 3.01 (d, *J* = 17.2, 11.2 Hz, 1H, Pz-H). ¹³C NMR (100 MHz, CDCl₃): δ 159.25 (Pz-C), 141.26 (Ph-C), 135.83 (Ph-C), 133.27 (Ph-C), 128.87 (Ph-C), 128.80 (Ph-C), 128.01 (Ph-C), 126.62 (Ph-C), 74.41 (Cp-C), 70.81 (Cp-C), 70.59 (Cp-C), 69.59 (Cp-C), 68.40 (Cp-C), 67.61 (Cp-C), 64.55 (Pz-C), 45.27 (Pz-C). MS (ESI) *m/z*: [M + H] 471.00, [M⁺] calcd. 470.36. Anal. calcd. for

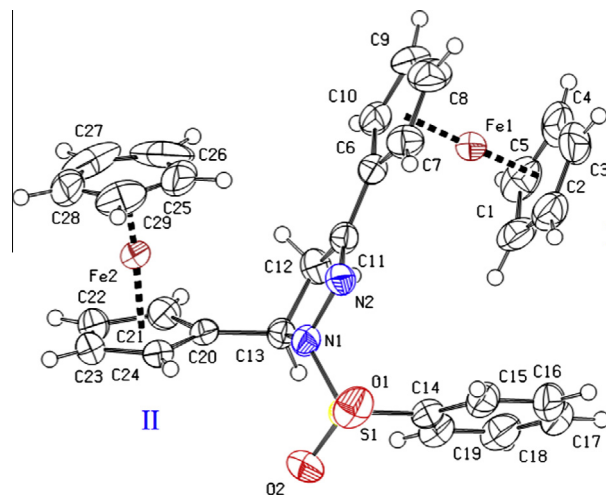


Fig. 1a. ORTEP view of **3a** (50% probability level), I and II refer to the two ferrocenyl units.

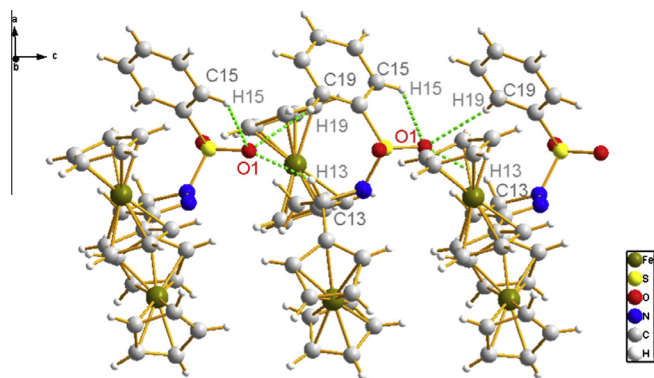


Fig. 1b. Hydrogen bonds between adjacent molecules of **3a**.

$C_{25}H_{22}FeN_2O_2S$: C 63.72, H 4.82, N, 5.95; found: C 63.84, H 4.71, N 5.96.

Results and discussion

Crystal structure of **3a–c**

Fig. 1a shows the molecule structure of **3a**, indicates that **3a** crystallizes in monoclinic crystal system, space group $P21/c$. Selected bond distances and angles are included in Tables S1 and S2. The structure consists of a benzenesulfonyl substituted pyrazole ring and two ferrocenes, attached to C11 and C13. The five atoms of the pyrazole ring are almost in the same plane. Their bond lengths tend to conjugate (C11–C12 bond: 1.489 Å; N1–N2 bond: 1.433 Å; C11=N2 bond: 1.306 Å). The Cp ring (C6–C10) of ferrocenyl unit I is almost parallel to the pyrazole ring (dihedral angle 4.56°), indicating that there is a conjugation among them. The bond length of C6–C11 (1.456 Å) is greater than a regular C=C double bond but shorter than a C–C single bond [17]. The two Cp rings of ferrocenyl unit I are eclipsed (pseudo-torsion angles of C1–Cg–Cg–C6: 4.21°) [33], while the two Cp rings of ferrocenyl unit II are halfway between eclipsed and staggered (pseudo-torsion angles of C20–Cg–Cg–C25: 19.60°). Coplanarity of the substituted Cp ring (C6–C10) of ferrocenyl unit I and pyrazole ring in **3a** has an impact on intramolecular forces. The crystal packing of

Table 2
H-bonding geometry (Å, °) for **3a–b**.

	Type	D–H (Å)	H···A (Å)	D···A (Å)	D–H···A (°)	
3a	C15–H15···O1	Intra.	0.95	2.48	2.85(8)	104
	C13–H13···O1	Inter.	1.00	2.38	3.22(3)	141
	C19–H19···O1	Inter.	0.96	2.51	3.31(3)	142
3b	C5–H5···O1	Inter.	0.93	2.59	3.43(9)	151
	3c	C13–H13···O1	Inter.	0.97	2.58	3.50(1)
C25–H25···O1		Inter.	0.92	2.52	3.38(2)	152

Table 3
Distances (Å) and angles (π) of C–H··· π contacts for **3a–b**.

		H··· π (Å)	C–H··· π (°)
3a	C8–H8···Cg ^a	2.74	141
	C1–H1···Cg ^b	2.85	143
	C23–H23···Cg ^c	2.65	150
3b	C10–H10···Cg ^d	2.98	139
	C25–H25···Cg ^e	2.85	98
3c	C16–H16···Cg ^f	2.87	127
	C4–H4···Cg ^g	2.96	167
	C21–H21···Cg ^h	2.77	97

^a Cg: (Cp ring of **3a** C20–C24).

^b Cg: (Cp ring of **3a** C25–C29).

^c Cg (Ph ring of **3a**).

^d Cg: (Ph ring of **3b** C20–25).

^e Cg (Pz ring of **3b**).

^f Cg: (Cp ring of **3c** C1–C5).

^g Cg: (Ph ring of **3c** C20–C25).

^h Cg: (Pz ring of **3c**).

3a (Fig. 1b) shows that molecules are linked into a one-dimensional chain along the c axis by intermolecular hydrogen bonding interactions and C–H··· π contacts (Tables 2 and 3). Interactions of molecules lead to a stable spatial structure by parallel stacking (Fig. 1c).

Different from **3a**, **3b** or **3c** contains only one ferrocenyl unit, however, three compounds are similar on the spatial structure (Figs. 2 and 3). The plane of the pyrazole ring of **3b** has a larger degree of distortion than in **3c**. However, the dihedral angles between the Cp ring (C6–C10) of ferrocenyl unit and pyrazole ring are small (12.48° for **3b**; 4.13° for **3c**). Compared with our previous

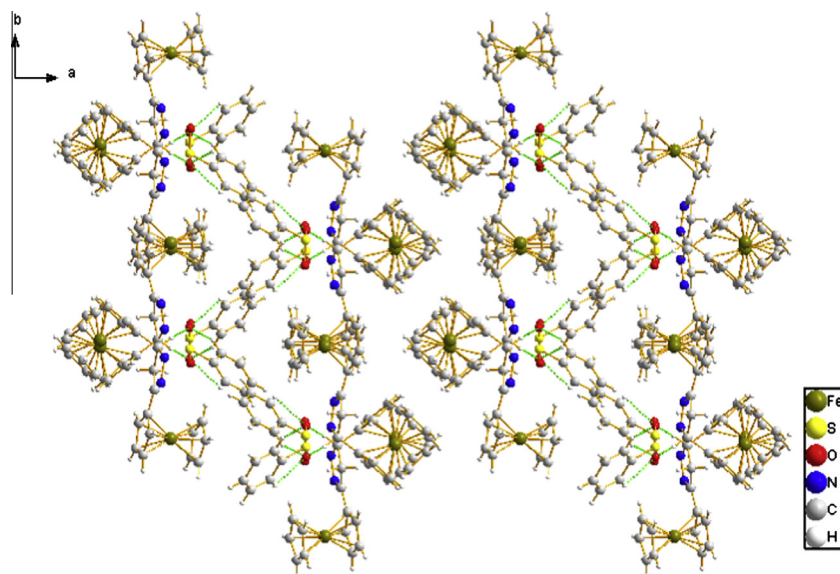
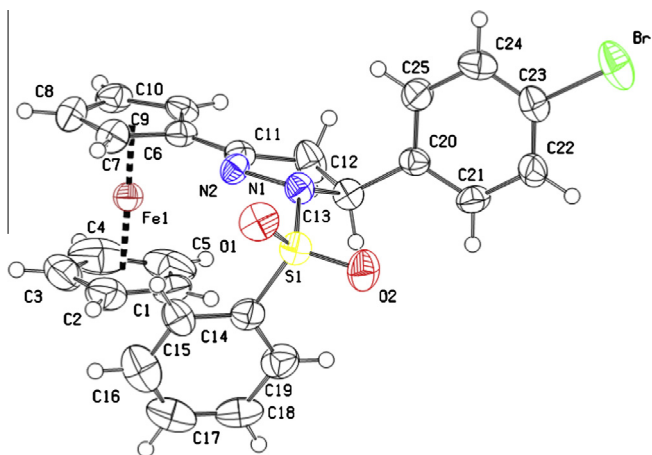
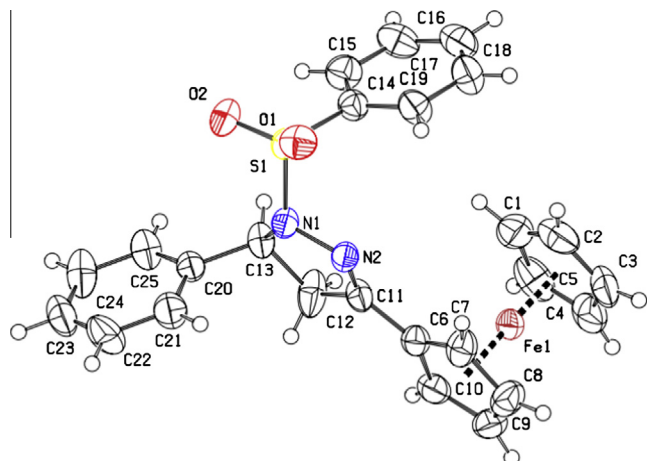


Fig. 1c. Cell packing diagram of **3a**, viewed down the c axis.

Fig. 2. ORTEP view of **3b** (50% probability level).Fig. 3. ORTEP view of **3c** (50% probability level).

work [34], bond lengths and angles of pyrazole ring and benzene-sulfonyl group in **3b** and **3c** are similar to those observed in **3a** (Tables S1 and S2). In the crystal lattices of both **3b** and **3c** molecules are associated through hydrogen bonds to form a spiral one-dimensional structure (Fig. S2) and held together by C—H... π contacts and stacked along the *a* axis (Fig. S3). The related data of hydrogen bonds and C—H... π contacts are also given in Tables 2 and 3.

Electrochemical behavior of **3a–c**

In the electrochemical analysis, the redox properties of **3a–c** ($c = 10^{-3}$ mol/L) are studied by cyclic voltammetry (CV) and differential pulse voltammetry (DPV). The electrochemical process of ferrocenyl moieties could be assigned as electrochemically quasi-reversible. Two redox peak potentials (\bar{E}_p) of **3a** (Fig. 4a and Table 4), for electrochemically reversible process are observed at 0.522 V and 0.664 V. The \bar{E}_p of **3b** and **3c** are 0.652 V and 0.669 V, respectively. All of them are higher than that of ferrocene (0.458 V). Simultaneously, the potential difference of anodic oxidation and cathodic reduction (ΔE) of **3a** for two ferrocenyl unit **I** and **II** were observed at 0.083 V and 0.081 V, the ΔE of **3b** and **3c** were 0.080 V and 0.076 V, respectively, and all of them are identical with ferrocene (0.075 V), which can confirm the electrochemical reversible oxidation process of ferrocenyl units of **3a–c**.

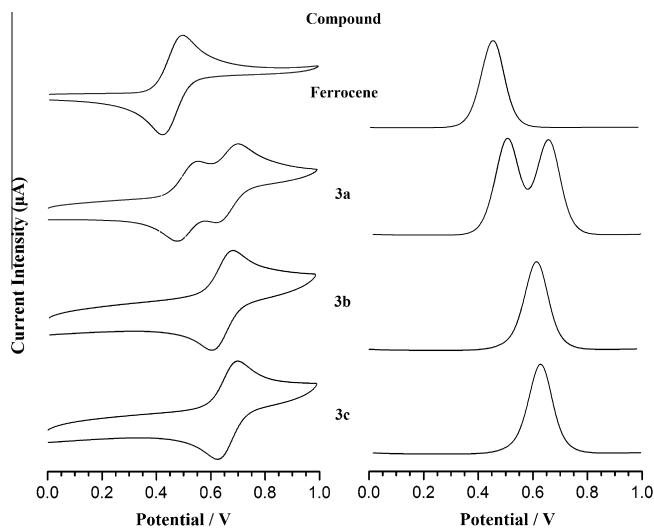
Fig. 4a. Cyclic voltammetry of ferrocene and **3a–c** at a scan rate of 0.1 V/s.

Table 4

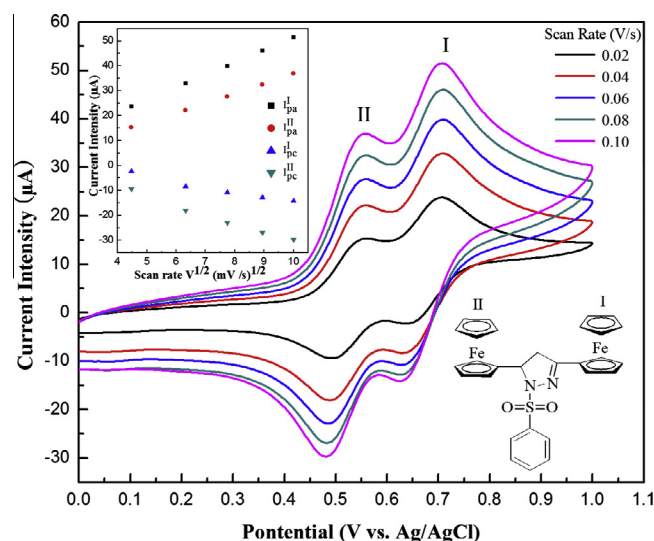
Cyclic voltammograms datas of ferrocene and **3a–c**.

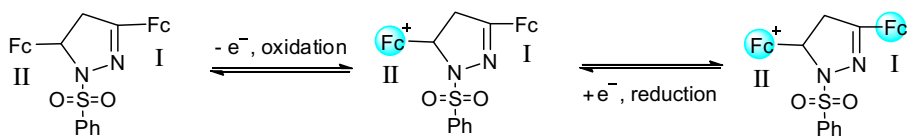
Compound	E_{pa} (V)	E_{pc} (V)	\bar{E}_p (V)	ΔE (V)	$\Delta\bar{E}_p$ (V)
Ferrocene	0.496	0.421	0.458	0.075	
3a, Fc unit I	0.706	0.623	0.664	0.083	0.142
3a, Fc unit II	0.562	0.481	0.522	0.081	
3b	0.690	0.610	0.652	0.080	
3c	0.707	0.631	0.669	0.076	

E_{pa} : anodic oxidation potential; E_{pc} : cathodic reduction potential; \bar{E}_p : redox peak potential;

$\bar{E}_p = (E_{pa} + E_{pc})/2$; $\Delta E = E_{pa} - E_{pc}$; $\Delta\bar{E}_p(\mathbf{3a}) = \bar{E}_p(\mathbf{3a}_{Fc(I)}) - \bar{E}_p(\mathbf{3a}_{Fc(II)})$.

The monoferrocenyl pyrazole **3b** and **3c** show only one ferrocenyl oxidation in their CV spectra. The oxidation potential of ferrocenyl group of the *p*-bromophenyl substituted pyrazole **3b** (0.690 V) is lower than that of the phenyl-substituted pyrazole ring **3c** (0.707 V), indicating a lower degree of electronic interaction between the ferrocenyl unit and pyrazole core than **3c**. It was in congruent with that the pyrazole ring and Cp ring (C6–C10) of **3c** had a higher degree of conjugated system than that of **3b**.

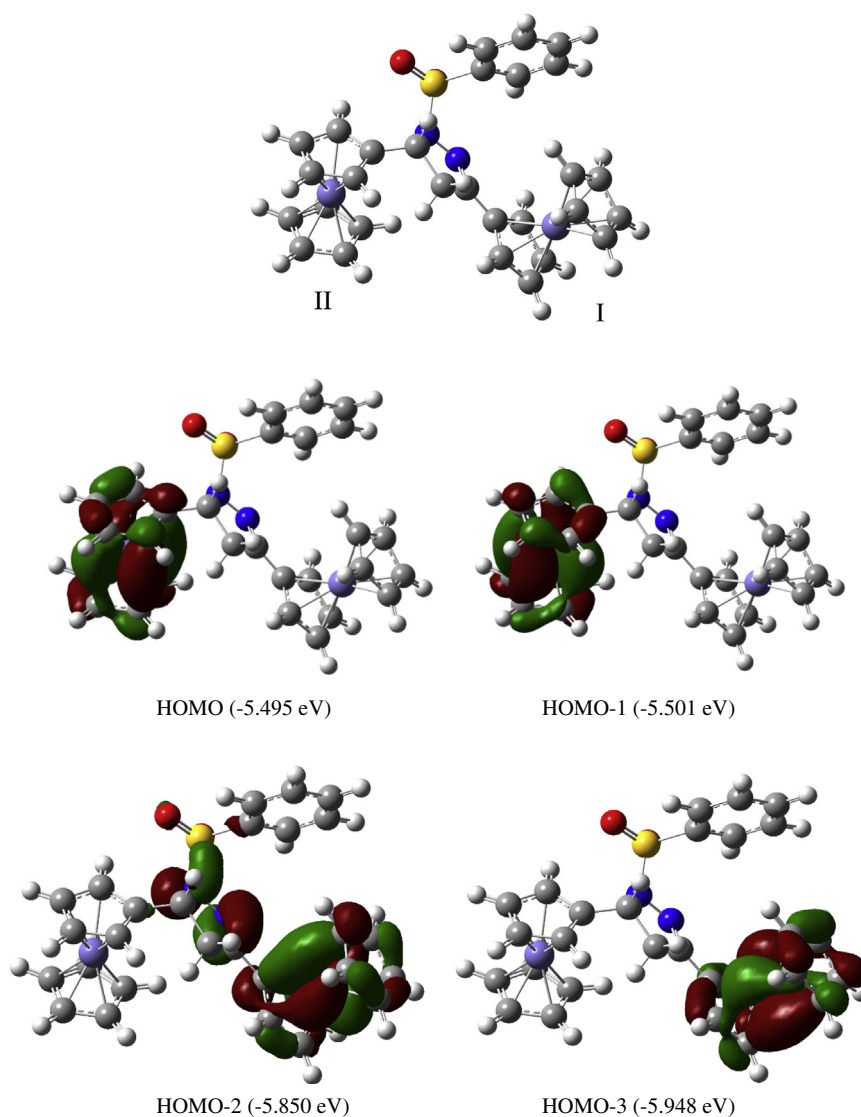
Fig. 4b. Cyclic voltammetry of **3a** at scan rates of 0.02, 0.04, 0.06, 0.08 and 0.1 V/s.

Scheme 2. Electron transfer mechanism of **3a**.

Analysis of the CV of **3a**, two ferrocenyl units, monoferrocenyl pyrazoles **3b** and **3c**, varying from 0.02 to 0.10 V/s, indicates a diffusion-controlled process (Fig. 4b). Both the anodic and cathodic peak currents are linear with the square root of scan rates ($v^{1/2}$). **3a** undergoes two successive reversible one-electron-oxidation processes. The potential difference of two redox peaks (ΔE_p) of ferrocenyl unit **I** and **II** is 0.142 V. The potential of the second wave ($\bar{E}_p = 0.664$ V) of **3a** and oxidation peak potential of **3b** ($\bar{E}_p = 0.610$ V), **3c** ($\bar{E}_p = 0.631$ V) occur at nearly the same location (Fig. 4a), the phenomenon manifesting that the redox couple is assigned to ferrocenyl unit **II**. The electrochemical behavior process of **3a** is viewed in Scheme 2. The first oxidation step occurs on ferrocenyl unit **II** at E_{pa} of 0.562 V, then the second redox wave of unit **I** emerges at $E_{pa} = 0.706$ V.

DFT study on electron transfer

In order to propose the electron transfer mechanisms and electrochemical inequivalence of two ferrocenyl units in **3a**, the molecular frontier orbitals of **3a** (Fig. 5) was exhibited by means of simplified theoretical modeling. Quantization calculation shows that ferrocenyl Cp rings are rich in negative charges and the iron atom is positive charged. In addition, a large number of positive charges are also enriched in S and C11 (Table S3). The ferrocenyl unit **II**, with HOMO (-5.495 eV) and HOMO-1 (-5.501 eV), tend to lose an electron faster than the ferrocenyl unit **I**, with HOMO-2 (-5.850 eV) and HOMO-3 (-5.948 eV). Thus, the ferrocenyl unit **II** is more inclined to serve as an electron donor than the ferrocenyl unit **I**. This result indicates that ferrocenyl unit **II** oxidizes first, in

Fig. 5. The structure of **3a** optimized by theoretical calculations and energy diagram of the first four HOMOs of **3a**.

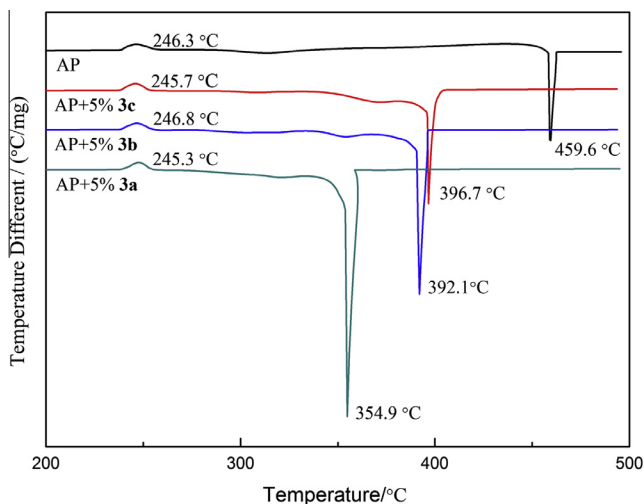


Fig. 6. DSC curves of AP, AP + 5% **3a**, AP + 5% **3b** and AP + 5% **3c**.

consistency with the electrochemical analysis that the first redox wave is associated with the oxidation of ferrocenyl unit **II** (Fig. 4a).

Catalytic effect on the decomposition of ammonium perchlorate (AP)

The decomposition of AP, affected by the catalytic burning rate, is analyzed using DSC curves (Fig. 6) and TG curves (Fig. S3). The DSC curves of AP shows that the additives **3a–c** (245.3 °C, 246.8 °C and 246.5 °C, respectively) have little effect on the crystallographic transition temperature of AP (246.3 °C) from orthorhombic form to cubic form [35,36]. After the addition of **3a–c**, the exothermic peaks become sharper, indicating the decomposition process of AP becomes more quickly. The result suggests that **3a–c** have a promoting effect on thermal decomposition of AP. The original exothermic peak of pure AP appears at 459.6 °C, and shift to a lower temperature (354.9 °C, 392.1 °C, 396.7 °C) when **3a–c** are mixed, respectively. The TG curves indicates that temperatures of initial thermal decompositions of four samples (pure AP and AP with **3a–c** additives) are between 280 and 285 °C, while that of complete decomposition temperatures are 459.6 °C, 354.9 °C, 396.3 °C, 403.9 °C, respectively. Specifically, **3a** shows a greater catalytic effect on the decomposition temperature of AP than **3a** and **3b**. This indicates that the catalytic effect on AP of dinuclear ferrocenyl pyrazole is more effective than mononuclear ferrocenyl pyrazole, which is due to the pyrazole substituent on the Cp ring of dinuclear ferrocenyl moiety, the bulky substituent can hinder the migration in AP. Combined with our earlier work, dinuclear ferrocene-based acyl dihydropyrazole only lower the thermal decomposition temperature by 74.3 °C [27], the sulfonyl substituent added to the dinuclear ferrocene-based dihydropyrazole ring could lower the thermal decomposition temperature (104.7 °C) than acyl substituent, which indicating that the sulfonyl substituent has significance in overcoming migration and evaporation of catalyst. The results and arguments confirm dinuclear ferrocenyl dpyrazole **3a** has a promoting effect on thermal decomposition of AP.

Conclusions

Three ferrocene-based sulfonyl dihydropyrazole derivatives have been synthesized, characterized, and investigated in spectral, electrochemistry and theoretical calculations (DFT). The X-ray crystallography of **3a** indicates that the pyrazole rings are almost coplanar with the Cp rings (C6–C10) of ferrocenyl unit **I**, forming

a large conjugated system. Adjacent molecules are connected by the hydrogen bonding to present a stable spatial structure. The cyclic voltammetry shows that the two quasi-reversible oxidation waves of **3** are diffusion-controlled. Specifically with **3a**, ferrocenyl unit **II** is more electron rich to serve as an electron donor than ferrocenyl unit **I**, further confirmed by DFT calculation. The results from DTA and TG analysis indicate that **3a–c** is of high catalytic effect on lowering the decomposition temperature of AP (by 62.9–104.7 °C) with 5 wt% addition of each. Experimental results show that the sulfonyl substituent added to the dihydropyrazole ring could lower the thermal decomposition temperature of AP. Meanwhile, dinuclear ferrocenyl substituted further reduces the migration and evaporation due to its steric hindrance. We expect that the novel dinuclear ferrocenyl pyrazole derivatives would be more widely used in high burning rates solid propellants.

Acknowledgements

We are grateful for the financial support from the National Natural Science Foundation of China (No. 21172036) and the Research Fund for the Doctoral Program of Higher Education of China (No. 20113514110002).

Appendix A. Supplementary material

Hydrogen bonds between adjacent molecules of **3b** and **3c** were given in Fig. S1. Cell packing diagram of **3b** and **3c** were given in Fig. S2. TG curves of AP, AP+5% **3a**, AP+5% **3b** and AP+5% **3c** were given in Fig. S3. Selected bond lengths for **3a–c** were given in Table S1. Selected angle between two bonds for **3a–c** were given in Table S2. Atomic natural charge of molecules **3a–c** were given in Table S2. Crystallographic data for the structures reported in this paper has been deposited with the Cambridge Crystallographic Data Centre as supplementary publications No. CCDC 800549 (**3a**), CCDC 985889 (**3b**) and CCDC 985981 (**3c**). Copies of the data can be obtained free of charge on application to CCDC, 12 Union Road, Cambridge CB2 1EZ, UK (fax: +44 1223 336 033; e-mail: deposit@ccdc.cam.ac.uk or <http://www.ccdc.cam.ac.uk>). Supplementary data associated with this article can be found, in the online version, at <http://dx.doi.org/10.1016/j.molstruc.2014.03.013>.

References

- [1] I. Damljanovic, M. Vukicevic, N. Radulovic, R. Palic, E. Ellmerer, Z. Ratkovic, M.D. Joksovic, R.D. Vukicevic, *Bioorg. Med. Chem. Lett.* 19 (2009) 1093–1096.
- [2] X.F. Huang, J.F. Tang, J.L. Ji, X.L. Wang, B.F. Ruan, *J. Organomet. Chem.* 706–707 (2012) 113–123.
- [3] M.D. Joksovic, V. Markovic, Z.D. Juranic, T. Stanojkovic, L.S. Jovanovic, I.S. Damljanovic, K.M. Szécsényi, N. Todorovic, S. Trifunovic, R.D. Vukicevic, *J. Organomet. Chem.* 694 (2009) 3935–3942.
- [4] Z. Ratkovic, Z.D. Juranic, T. Stanojkovic, D. Manojlovic, R.D. Vukicevic, N. Radulovic, M.D. Joksovic, *Bioorg. Chem.* 38 (2010) 26–32.
- [5] S.L. Shen, J. Zhu, M. Li, B.X. Zhao, J.Y. Miao, *Eur. J. Med. Chem.* 54 (2012) 287–294.
- [6] Y.S. Xie, X.H. Pan, B.X. Zhao, J.T. Liu, D.S. Shin, J.H. Zhang, L.W. Zheng, J. Zhao, J.Y. Miao, *J. Organomet. Chem.* 693 (2008) 1367–1374.
- [7] Y.S. Xie, H.L. Zhao, H. Su, B.X. Zhao, J.T. Liu, J.K. Li, H.S. Lv, B.S. Wang, D.S. Shin, J.Y. Miao, *Eur. J. Med. Chem.* 45 (2010) 210–218.
- [8] J. Cody, S. Mandal, L. Yang, C.J. Fahmi, *J. Am. Chem. Soc.* 130 (2008) 13023–13032.
- [9] I. Damljanovic, M. Čolović, M. Vukicevic, D. Manojlovic, N. Radulovic, K. Wurst, G. Laus, Z. Ratkovic, M. Joksovic, R.D. Vukicevic, *J. Organomet. Chem.* 694 (2009) 1575–1580.
- [10] K.Y. Zhang, S.P. Li, N. Zhu, I.W. Or, M.S. Cheung, Y.W. Lam, K.K. Lo, *Inorg. Chem.* 49 (2010) 2530–2540.
- [11] T. Amanpour, P. Mirzaei, A. Bazgir, *Tetrahedron Lett.* 53 (2012) 1421–1423.
- [12] H. He, J. Xia, G. Chang, X. Peng, Z. Lou, K. Nakatani, X. Zhou, S. Wang, *Biosens. Bioelectron.* 42 (2013) 36–40.
- [13] B.T. Zhao, L.W. Liu, X.C. Li, G.R. Qu, E. Belhadji, F.L. Derf, M. Sallé, *Tetrahedron Lett.* 54 (2013) 23–26.
- [14] Z.M. Li, S.H. Xie, J.G. Zhang, J.L. Feng, K. Wang, T.L. Zhang, *J. Chem. Eng. Data* 57 (2012) 729–736.

- [15] J.S. Thompson, L. Zhang, J.P. Wyre, D. Brill, Z. Li, *Organometallics* 31 (2012) 7884–7892.
- [16] H.D. Li, Z.H. Ma, K. Yang, L.L. Xie, Y.F. Yuan, J. *Mol. Struct.* 1024 (2012) 40–46.
- [17] B. Wei, Y. Gao, C.X. Lin, H.D. Li, L.L. Xie, Y.F. Yuan, *J. Organomet. Chem.* 696 (2011) 1574–1578.
- [18] N. Dilsiz, A. Ünver, *J. Appl. Polym. Sci.* 101 (2006) 2538–2545.
- [19] K. Subramanian, *J. Polym. Sci., Part A: Polym. Chem.* 37 (1999) 4090–4099.
- [20] M.B. Talawar, R. Sivabalan, T. Mukundan, H. Muthurajan, A.K. Sikder, B.R. Gandhe, A.S. Rao, *J. Hazard. Mater.* 161 (2009) 589–607.
- [21] R. Wang, Y. Guo, Z. Zeng, B. Twamley, J.N.M. Shreeve, *Chem. Eur. J.* 15 (2009) 2625–2634.
- [22] H. Yu, L. Wang, J. Huo, J. Ding, Q. Tan, *J. Appl. Polym. Sci.* 110 (2008) 1594–1599.
- [23] G. Duan, X. Yang, J. Chen, G. Huang, L. Lu, X. Wang, *Powder Technol.* 172 (2007) 27–29.
- [24] Y. Wang, J. Zhu, X. Yang, L. Lu, X. Wang, *Thermochim. Acta* 437 (2005) 106–109.
- [25] X.J. Feng, S.M. Min, P. Lei, L.J. Yun, Z.C. Jun, *J. Inorg. Organomet. Polym.* 21 (2011) 175–181.
- [26] G. Cin, S. Demirel Topel, A. Cakıcı, A. Yıldırım, A. Karadağ, *J. Chem. Crystallogr.* 42 (2012) 372–380.
- [27] Y. Gao, H.D. Li, C.F. Ke, L.L. Xie, B. Wei, Y.F. Yuan, *Appl. Organomet. Chem.* 25 (2011) 407–411.
- [28] D. Saravanakumar, N. Sengottuvelan, V. Narayanan, M. Kandaswamy, T.L. Varghese, *J. Appl. Polym. Sci.* 119 (2011) 2517–2524.
- [29] F. Xiao, X. Sun, X. Wu, J. Zhao, Y. Luo, *J. Organomet. Chem.* 713 (2012) 96–103.
- [30] G.M. Sheldrick, *Acta Crystallogr., Sect. A: Found. Crystallogr.* 64 (2008) 112–122.
- [31] M. Frisch, G. Trucks, H. Schlegel, G. Scuseria, M. Robb, J. Cheeseman, J. Montgomery Jr., T. Vreven, K. Kudin, J. Burant, Inc., Wallingford CT, 2004.
- [32] P.J. Stephens, F.J. Devlin, C.F. Chabalowski, M.J. Frisch, *J. Phys. Chem.* 98 (1994) 11623–11627.
- [33] T. Klimova, E.I. Klimova, M.M. García, J.M. Méndez Stivalet, L. Rúa Ramrez, *J. Organomet. Chem.* 633 (2001) 137–142.
- [34] C.Y. Li, J.B. Zhuo, L.L. Xie, H.D. Li, W.F. Wang, Y.F. Yuan, *Chem. J. Chin. Univ.* 32 (2011) 1305–1311.
- [35] A.A. Said, R. Al-Qasbi, *Thermochim. Acta* 275 (1996) 83–91.
- [36] S. Vyazovkin, C.A. Wight, *Chem. Mater.* 11 (1999) 3386–3393.